Cooperative Transportation of a Payload using Quadrotors: a Reconfigurable Cable-Driven Parallel Robot

Carlo Masone, Heinrich H. Bülthoff and Paolo Stegagno

***Abstract*— This paper addresses the problem of cooperative aerial transportation of an object using a team of quadrotors. The approach presented to solve this problem accounts for the full dynamics of the system and it is inspired by the literature on reconfigurable cable-driven parallel robots (RCDPR). Using the modelling convention of RCDPR it is derived a direct relation between the motion of the quadrotors and the motion of the payload. This relation makes explicit the available internal motion of the system, which can be used to automatically achieve additional tasks. The proposed method does not require to specify a priory the forces in the cables and uses a tension distribution algorithm to optimally distribute them among the robots. The presented framework is also suitable for online teleoperation. Physical simulations and real experiments with a human-in-the-loop validate the proposed approach.**

I. INTRODUCTION

In this paper we consider the task of cooperative aerial transportation and manipulation of an object using a team of quadrotors. In particular, we study the case of a payload suspended via cables (see Fig. 1) because: 1) the use of cables removes the need to carry manipulators or grippers onboard the quadrotors, thus allowing to transport heavier objects, and 2) cables can have a long extension, thus giving more freedom to distribute the quadrotors.

The problem of cooperative manipulation of a payload suspended via cables by quadrotors or other unmanned aerial vehicles (UAVs) has already been addressed in several recent publications, [1], [2], [3], [4], [5], however these papers are based on a quasi-static model of the system and neglect the dynamics of the payload. In [6] the authors study the problem of cooperative maniptulation of a load suspended by quadrotors via cables, and the solution proposed is based on the full dynamics of the system. he authors prove that the system is differentially flat and give an expression of the flat output, using it to plan feasible trajectories. However, that approach has a few drawbacks: 1) it requires to specify the trajectory of the load up to the sixth derivative in position and up to the fourth derivative in orientation, which does not lend itself to including a human piloting the payload online; 2) to resolve the internal forces of the system it is necessary to specify some components of the cable forces up to the fourth derivative, but this is not intuitive and it is unclear the effect of this choice on the trajectories of the quadrotors; 3) the flat output does not give a direct and explicit understanding of the trajectories of the quadrotors, which can only be obtained by integrating the input.

C. Masone, H. H. Bülthoff and P. Stegagno are with the Max Planck Institute for Biological Cybernetics, Spemannstraße 38, 72076 Tübingen, Germany {carlo.masone,hhb,paolo.stegagno}@tuebingen.mpg.de.

H. H. Bülthoff is also with the Department of Brain and Cognitive Engineering, Korea University, Seoul, 136-713 Korea.

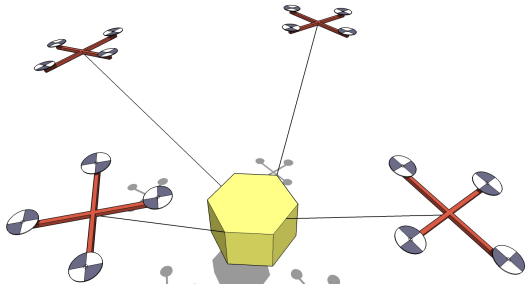

Fig. 1: Sketch of the system.

In this paper we present a different approach to solve this problem while taking into account the full dynamics of the system. Our solution is inspired by recent works on reconfigurable cable-driven parallel robots (RCDPRs) on [7], [8], [9], [10]. We recall that RCDPRs are a special category of cable driven parallel robots in which the actuators pulling the cables (in our case quadrotors, more in general winches) possess some degrees of freedom to move in space. Following the modelling convention of RCDPRs we are able to find a direct relation between motion of the payload and motion of the quadrotors. Such relation can be used to specify internal motions of the robots in order to automatically achieve some desirable task, as for example a smooth distribution of the load among the robots. Furthermore the proposed approach does not require to specify a priori non intuitive references for some of the internal forces, but rather optimizes them online by using a tension distribution algorithm. Lastly, we believe that our approach is more suitable than the method described in [6] for a teleoperation framework with a human piloting the payload.

In addition to the aforementioned contribution to the field of cooperative aerial transportation, this paper constitutes also a contribution to the RCDPRs field. In fact, all recent works [7], [8], [9], [10] have considered only the static kinematics of RCDPRs, using it to find the optimal actuators configuration according to various metrics. Yet none of these papers fully considers the effect of the motion of the actuators on the payload. In this paper we describe, to the best of our knowledge for the first time, the differential kinematics of a generic RCDPR and we show explicitly the relation between the motion of the actuators and the motion of the payload. We also describe the nature of the internal motions by means of a spatial decomposition of the motion of the actuators. Finally, we show how the motion of the

actuators of a RCDPR can be used online to control the motion of the payload.

The rest of the paper, is organized as follows. In Sec. II we introduce the system and few modelling assumptions. Then in Sec. III we derive a differential kinematics model of the system, highlighting the nature of the internal motions and the connection to CDPRs. The dynamics of the payload and quadrotors are described in Sec. IV and a trajectory controller is designed in Sec. V. Finally, in Sec. VI we present experimental results to validate our findings.

II. Preliminaries

In this paper we consider the system depicted in Fig. 1, that is composed of:

1) a rigid body (*payload*), tasked to follow a trajectory in a n-dimensional task space, with $n \leq 6$[1];
2) $m \geq n$ quadrotors that are connected to the payload via cables (one cable per UAV)[2].

The i-th cable is attached at one end to a point B_i on the payload (*onboard connection*) and at the other end it is attached to point as A_i on the quadrotor (*moving anchor*). To model this system we will make the following assumptions:

A1) The anchor A_i is coincident with the center of mass of the i-th quadrotor.

A2) The cables are massless, inextensible and they are always taut (constant cable length).

Assumption A1) is reasonable, see also [6], because the mass of the cables is presumably significantly smaller than the mass of the payload and the elasticity of the cables is negligible. Instead A2) is verified if we guarantee that the cable tensions are kept in a suitable (positive) range, which will be discussed in Sec. V

With this setting we will tackle the problem of steering the payload along the desired trajectory in three steps:

Kinematics: We study the differential kinematics of the system and derive a mapping between motion of the payload and motion of the anchors. This mapping is used to translate the desired trajectory of the payload into a reference trajectory for the quadrotors.

Dynamics: We describe the dynamics of the system, showing explicitly the interaction between payload and UAVs through the cable forces. This model is used to determine the required cable tensions for the desired payload dynamics.

Control: We design a trajectory tracking controller that, using the kinematic and dynamic models previously introduced, computes the inputs for the quadrotors.

III. Kinematics

The pose of the payload is described by the vector $\boldsymbol{x}_{\boldsymbol{\nu}} = [{}^W\boldsymbol{p}^T \;\; \boldsymbol{\nu}^T]^T \in SE(3)$ that represents position ${}^W\boldsymbol{p} \in \mathbb{R}^3$ and orientation $\boldsymbol{\nu} \in SO(3)$ of a frame $\mathcal{F}_L = \left\{\mathcal{O}_L, \vec{\mathcal{X}}_L, \vec{\mathcal{Y}}_L, \vec{\mathcal{Z}}_L\right\}$ fixed on the load w.r.t. an inertial world frame $\mathcal{F}_W = \left\{\mathcal{O}_W, \vec{\mathcal{X}}_W, \vec{\mathcal{Y}}_W, \vec{\mathcal{Z}}_W\right\}$ (see Fig. 2). Hereinafter we describe the orientation using the roll-pitch-yaw angles $\boldsymbol{\nu} = (\phi\ \theta\ \psi)^T$ and the rotation matrix from $\mathcal{F}_L$ to $\mathcal{F}_W$, i.e., ${}^W R_L$. Velocity and acceleration of the payload are denoted as $\dot{\boldsymbol{x}} = [{}^W\dot{\boldsymbol{p}}^T \;\; \boldsymbol{\omega}^T]^T$ and $\ddot{\boldsymbol{x}} = [{}^W\ddot{\boldsymbol{p}}^T \;\; \dot{\boldsymbol{\omega}}^T]^T$, where $\boldsymbol{\omega}$ and $\dot{\boldsymbol{\omega}}$ are the angular velocity and acceleration of the rigid body in $\mathcal{F}_W$[3]. The position of the end-point of the i-th cable, i.e. the moving anchor A_i, is described in $\mathcal{F}_W$ by the vector ${}^W\boldsymbol{a}_i \in \mathbb{R}^3$ (see Fig. 2). The position vectors of all the anchors can be stacked together in the more compact representation $\boldsymbol{\chi} = \begin{bmatrix} {}^W\boldsymbol{a}_1^T & \cdots & {}^W\boldsymbol{a}_m^T \end{bmatrix}^T \in \mathbb{R}^{3m}$.

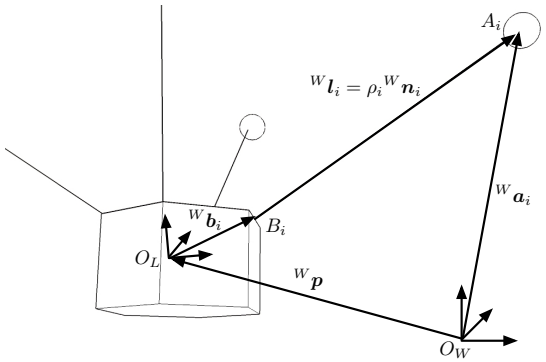

Fig. 2: System kinematics.

Our goal is to find a kinematic model that relates $\boldsymbol{x}_{\boldsymbol{\nu}}$, $\dot{\boldsymbol{x}}$ and $\ddot{\boldsymbol{x}}$ to $\boldsymbol{\chi}$, $\dot{\boldsymbol{\chi}}$ and $\ddot{\boldsymbol{\chi}}$.

Remark 1. In the kinematics we refer only to the anchors A_i where the cables are connected, not to the quadrotors. The quadrotors providing the actuation of the anchors are only considered in the dynamics.

Remark 2. In this paper we only consider the motion of the payload and of the anchors up to their acceleration ($\ddot{\boldsymbol{x}}$ and $\ddot{\boldsymbol{\chi}}$) because this is enough for the purpose of our controller. Nevertheless, the discussion presented in this section extends seamlessly to higher order derivatives.

Under assumption $A2$) in Sec. II the generic i-th cable satisfies a loop closure constraint that is given by a triangle with vertices i) the moving anchor A_i, ii) the onboard connection B_i, and iii) the point O_L (see Fig. 2), i.e.

$$ {}^W\boldsymbol{l}_i = \rho_i {}^W\boldsymbol{n}_i = {}^W\boldsymbol{a}_i - {}^W\boldsymbol{p} - \underbrace{{}^W R_L {}^L\boldsymbol{b}_i}_{{}^W\boldsymbol{b}_i} \tag{1} $$

where

- ${}^L\boldsymbol{b}_i \in \mathbb{R}^3$ is the position of B_i in $\mathcal{F}_L$ and ${}^W\boldsymbol{b}_i = {}^W R_L {}^L\boldsymbol{b}_i$ is the vector of $\overrightarrow{O_L B_i}$ in $\mathcal{F}_W$;
- ${}^W\boldsymbol{l}_i \in \mathbb{R}^3$ is the vector from B_i to A_i expressed in $\mathcal{F}_W$ and it is factorized into the unit vector ${}^W\boldsymbol{n}_i \in \mathbb{R}^3$ (*cable direction* in $\mathcal{F}_W$) and the scalar $\rho_i > 0$ (*cable length*).

[1]The configuration space of the rigid body is $SE(3)$, but the task might not fully specify position and orientation of the load.

[2]Even though from a static analysis [2] three quadrotors are enough to suspend the payload in any configuration, to be able to apply any wrench to the load we need at least $m = n$ robots.

[3]Note that $\dot{\boldsymbol{x}}_{\boldsymbol{\nu}} \neq \dot{\boldsymbol{x}}$ since $\boldsymbol{\omega} \neq \dot{\boldsymbol{\nu}}$.

Equation (1) can be written for all the cables in the following compact form

$$N\boldsymbol{\rho} = \boldsymbol{\chi} - \boldsymbol{\xi}\,, \tag{2}$$

where

- $\boldsymbol{\rho} = \begin{bmatrix}\rho_1 & \cdots & \rho_m\end{bmatrix}^T \in \mathbb{R}^m$ is the vector of cable lengths;
- $\boldsymbol{\xi} = \mathbf{1}_{m\times 1}\otimes {}^W\boldsymbol{p} + \begin{bmatrix}{}^W\boldsymbol{b}_1^T & \cdots & {}^W\boldsymbol{b}_m^T\end{bmatrix}^T$ is the vector of stacked positions of the connection points B_i in $\mathcal{F}_W$[4];
- $N \in \mathbb{R}^{3m\times m}$ is the block diagonal matrix of cable directions, i.e.,

$$N = \begin{bmatrix} {}^W\boldsymbol{n}_1 & \mathbf{0}_{3\times 1} & \cdots & \mathbf{0}_{3\times 1} \\ \mathbf{0}_{3\times 1} & {}^W\boldsymbol{n}_2 & \cdots & \mathbf{0}_{3\times 1} \\ \mathbf{0}_{3\times 1} & \mathbf{0}_{3\times 1} & \ddots & \mathbf{0}_{3\times 1} \\ \mathbf{0}_{3\times 1} & \mathbf{0}_{3\times 1} & \dots & {}^W\boldsymbol{n}_m \end{bmatrix} \tag{3}$$

By differentiating (2) twice we have

$$\dot{N}\boldsymbol{\rho} = \dot{\boldsymbol{\chi}} - \dot{\boldsymbol{\xi}} \tag{4}$$

$$\ddot{N}\boldsymbol{\rho} = \ddot{\boldsymbol{\chi}} - \ddot{\boldsymbol{\xi}} \tag{5}$$

where we have imposed that $\dot{\boldsymbol{\rho}} = \ddot{\boldsymbol{\rho}} = \mathbf{0}_{m\times 1}$ (assumption of taut cables).

Equations (2), (4) and (5) provide the sought relation between motion of the anchors ($\boldsymbol{\chi}$, $\dot{\boldsymbol{\chi}}$ and $\ddot{\boldsymbol{\chi}}$) and motion of the payload (implicitly expressed by $\boldsymbol{\xi}$, $\dot{\boldsymbol{\xi}}$ and $\ddot{\boldsymbol{\xi}}$). However, from (4) and (5) it is not immediately clear how the motion of the anchors relates to the motion of the payload. To better understand this mechanism, we will make the dependency from $\dot{\boldsymbol{x}}$ and $\ddot{\boldsymbol{x}}$ explicit in (4) and (5) and we will decompose the trajectories into two vector spaces, that are:

- $\mathcal{R}(N)$, the m-dimensional range space of N.
- $\mathcal{K}(N)$, the $2m$-dimensional null space of N.

First, we need to introduce a property that is instrumental to achieve the aforementioned decomposition.

Lemma 1. The trajectories of the cable suspended payload with moving anchors and fixed length cables, with kinematics (2), (4) and (5), satisfy

$$N^T\dot{N}\boldsymbol{\rho} = \mathbf{0}_{m\times 1} \tag{6}$$

$$N^T\ddot{N}\boldsymbol{\rho} = \dot{\boldsymbol{N}}^T\left(\dot{\boldsymbol{\xi}} - \dot{\boldsymbol{\chi}}\right) \tag{7}$$

Proof. From the structure of N in (3), we have that

$$N^T\dot{N} = \begin{bmatrix} {}^W\boldsymbol{n}_1^T\,{}^W\dot{\boldsymbol{n}}_1 & 0 & \cdots & 0 \\ 0 & {}^W\boldsymbol{n}_2^T\,{}^W\dot{\boldsymbol{n}}_2 & \cdots & 0 \\ 0 & 0 & \ddots & 0 \\ 0 & 0 & \dots & {}^W\boldsymbol{n}_m^T\,{}^W\dot{\boldsymbol{n}}_m \end{bmatrix}$$

Since the time derivative of the generic unit vector ${}^W\boldsymbol{n}_i$ is ${}^W\dot{\boldsymbol{n}}_i = \boldsymbol{\omega}_{\boldsymbol{n}_i} \times {}^W\boldsymbol{n}_i$, with $\boldsymbol{\omega}_{n_i}$ being the angular velocity of the i-th cable, then it follows that ${}^W\boldsymbol{n}_i^T\,{}^W\dot{\boldsymbol{n}}_i = 0$ and consequently $N^T\dot{N} = \mathbf{0}_{m\times m}$, which proves (6).

[4]$\otimes$ is the Kronecker product operator and $\mathbf{1}_{m\times 1}$ is the $m \times 1$ matrix with all entries equal to 1.

To prove (7), isolate $\boldsymbol{\rho}$ on the l.h.s. of (2) by multiplying both sides for N^T. The expression thus obtained can be differentiated twice w.r.t. time, yielding

$$\begin{aligned}\ddot{\boldsymbol{\rho}} &= \ddot{N}^T(\boldsymbol{\chi} - \boldsymbol{\xi}) + 2\dot{N}^T\left(\dot{\boldsymbol{\chi}} - \dot{\boldsymbol{\xi}}\right) + N^T\left(\ddot{\boldsymbol{\chi}} - \ddot{\boldsymbol{\xi}}\right) \\ &= \ddot{N}^T N\boldsymbol{\rho} + 2\dot{N}^T\left(\dot{\boldsymbol{\chi}} - \dot{\boldsymbol{\xi}}\right) + N^T\ddot{N}\boldsymbol{\rho} = \mathbf{0}_{m\times 1}\end{aligned}$$

The block diagonal structure of N (see (3)) and $\ddot{N}$ implies that $\dot{N}^T N = N^T\dot{N}$, and using this property on the previous equation concludes the proof.

□

Finally, we can present the following result for the spatial decomposition of the trajectories of the anchors.

Propositon 1. For the cable suspended payload with fully movable anchors and fixed cable length, the kinematic mapping from payload velocity $\dot{\boldsymbol{x}}$ and acceleration $\ddot{\boldsymbol{x}}$ to anchors linear velocities $\dot{\boldsymbol{\chi}}$ and accelerations $\ddot{\boldsymbol{\chi}}$ is:

$$\dot{\boldsymbol{\chi}}_{\mathcal{R}} = NJ_{\mathcal{R}}\dot{\boldsymbol{x}} \tag{8}$$

$$\ddot{\boldsymbol{\chi}}_{\mathcal{R}} = NJ_{\mathcal{R}}\ddot{\boldsymbol{x}} + N\dot{N}^T\left(\dot{\boldsymbol{\xi}} - \dot{\boldsymbol{\chi}}\right) \tag{9}$$

$$\dot{\boldsymbol{\chi}}_{\mathcal{K}} = \dot{N}\boldsymbol{\rho} + J_{\mathcal{K}}\dot{\boldsymbol{x}} \tag{10}$$

$$\ddot{\boldsymbol{\chi}}_{\mathcal{K}} = \ddot{N}\boldsymbol{\rho} + J_{\mathcal{K}}\ddot{\boldsymbol{x}} - N\dot{N}^T\left(\dot{\boldsymbol{\xi}} - \dot{\boldsymbol{\chi}}\right) \tag{11}$$

where $\bullet_{\mathcal{R}}$ indicates a vector on $\mathcal{R}(N)$, $\bullet_{\mathcal{K}}$ indicates a vector on $\mathcal{K}(N)$, $\dot{\boldsymbol{\chi}} = \dot{\boldsymbol{\chi}}_{\mathcal{R}} + \dot{\boldsymbol{\chi}}_{\mathcal{K}}$, $\ddot{\boldsymbol{\chi}} = \ddot{\boldsymbol{\chi}}_{\mathcal{R}} + \ddot{\boldsymbol{\chi}}_{\mathcal{K}}$,

$$J_{\mathcal{R}} = N^T\begin{bmatrix} I_{3\times 3} & -[{}^W\boldsymbol{b}_1]_\times \\ \vdots & \vdots \\ I_{3\times 3} & -[{}^W\boldsymbol{b}_m]_\times \end{bmatrix} \tag{12}$$

$$J_{\mathcal{K}} = (I_{3m\times 3m} - NN^T)\begin{bmatrix} I_{3\times 3} & -[{}^W\boldsymbol{b}_1]_\times \\ \vdots & \vdots \\ I_{3\times 3} & -[{}^W\boldsymbol{b}_m]_\times \end{bmatrix} \tag{13}$$

and $[\bullet]_\times$ indicates the skew-symmetric matrix operator such $[\boldsymbol{v}_1]_\times \boldsymbol{v}_2 = \boldsymbol{v}_1 \times \boldsymbol{v}_2$ for $\boldsymbol{v}_1, \boldsymbol{v}_2 \in \mathbb{R}^3$.

Proof. Projection on $\mathcal{R}(N)$ The projection onto $\mathcal{R}(N)$ is obtained by premultiplying both sides of (4) and (5) for the orthogonal projection operator NN^T. Consider first (4). Using the notation $\dot{\boldsymbol{\chi}}_{\mathcal{R}} = NN^T\dot{\boldsymbol{\chi}}$ and property (6), it follows that

$$\dot{\boldsymbol{\chi}}_{\mathcal{R}} = NN^T\dot{\boldsymbol{\xi}}.$$

Since by definition

$$\dot{\boldsymbol{\xi}} = \begin{bmatrix} I_{3\times 3} & -[{}^W\boldsymbol{b}_1]_\times \\ \vdots & \vdots \\ I_{3\times 3} & -[{}^W\boldsymbol{b}_1]_\times \end{bmatrix}\dot{\boldsymbol{x}}$$

we verify (8) and (12). Consider now (5). Using the same procedure, with $\ddot{\boldsymbol{\chi}}_{\mathcal{R}} = NN^T\ddot{\boldsymbol{\chi}}$ and property (7), we obtain

$$\ddot{\boldsymbol{\chi}}_{\mathcal{R}} = NN^T\ddot{\boldsymbol{\xi}} + N\dot{N}^T\left(\dot{\boldsymbol{\xi}} - \dot{\boldsymbol{\chi}}\right)$$

As already observed before, it is easy to verify that $\boldsymbol{N}^T\ddot{\boldsymbol{\xi}} = N^TJ_{\mathcal{R}}\ddot{\boldsymbol{x}}$, thus proving (9)

Projection on $\mathcal{K}(N)$ The projection onto $\mathcal{K}(N)$ is obtained with the orthogonal null-space projection operator $(I_{3m\times 3m} - NN^T)$. Repeating the same procedure of the previous case, premultiplying (4) for the projection matrix and using the notation $\dot{\boldsymbol{\chi}}_{\mathcal{K}} = (I_{3m\times 3m} - NN^T)\dot{\boldsymbol{\chi}}$ and property (6) yields

$$\dot{\boldsymbol{\chi}}_{\mathcal{K}} = \dot{N}\boldsymbol{\rho} + (I_{3m\times 3m} - NN^T)\dot{\boldsymbol{\xi}} \,.$$

Once again, from the structure of $\dot{\boldsymbol{\xi}}$ it is trivial to see that $(I_{3m\times 3m} - NN^T)\dot{\boldsymbol{\xi}} = J_{\mathcal{K}}\dot{\boldsymbol{x}}$, proving (11) and (13). Lastly applying the projection on (5) and using (7) gives

$$\ddot{\boldsymbol{\chi}}_{\mathcal{K}} = \ddot{N}\boldsymbol{\rho} + \left(I_{3m\times 3m} - NN^T\right)\ddot{\boldsymbol{\xi}} - N\dot{N}^T\left(\dot{\boldsymbol{\xi}} - \dot{\boldsymbol{\chi}}\right)$$

which, for the previous considerations, verifies (11). □

Remark 3. The term $N\dot{N}^T\left(\dot{\boldsymbol{\xi}} - \dot{\boldsymbol{\chi}}\right)$ in (9) and (11) is the apparent acceleration due to the rotation of the cables represented by $\dot{N}$.

Remark 4 (*Internal Motions*)**.** In comparison to (4) and (5) Prop. 1 gives a better idea of the relation between motion of the anchors and motion of the payload. Proposition 1 states that, given the current state of the kinematic system, the motion of the payload uniquely defines the motion of the anchors on $\mathcal{R}(N)$, but not on $\mathcal{K}(N)$. The motion of the anchors on $\mathcal{K}(N)$ requires to additionally specify a derivative of N ($\dot{N}$ for $\dot{\boldsymbol{\chi}}_{\mathcal{K}}$ and $\ddot{N}$ for $\ddot{\boldsymbol{\chi}}_{\mathcal{K}}$). The interpretation of this fact is that only the motion of the anchors on $\mathcal{R}(N)$, i.e. along the the cables, instantaneously affects the motion of the payload whereas the $2m$ degrees of freedom of the anchors on $\mathcal{K}(N)$ can be used to assign internal motions that change the configuration of cables without moving the payload. These internal motions can be used, for example, to maximize the stiffness of the system or to group more densely the formation of robots when passing through narrow gaps. The development of such behaviours is outside the scope of this paper and it will be tackled in future studies. Nevertheless, in the experiments presented in Sec. VI we will show few basic examples of how to use the internal motions.

Remark 5 (*Forward Kinematics*)**.** The forward kinematics (2) cannot be uniquely solved with the payload pose, but it requires also the cable direction N. Therefore, (2) can be solved either with an optimization algorithm that implicitly chooses N according to some metric or by assigning N. In the experiments presented in Sec. VI we solve the forward kinematics by assigning the initial value N and then integrating it with the signals $\dot{N}$ and $\ddot{N}$ that are chosen to achieve a desired internal motion.

Remark 6 (*Comparison with CDPRs*)**.** The model presented here describes the differential kinematics of a RCDPR with freely moving anchors and the constraint of fixed cable lengths. Recently, few papers have addressed the topic of RCDPRs, [7], [8], [9], [10], yet without providing an analysis of the relation between motion of the anchors and motion of the payload. The common approach is to compute the position of the anchors by numerically solving the forward kinematics to maximize some metric, but this strategy is used only for reconfiguring the cables whereas the motion of the payload is achieved by changing the cable length. Here we directly use the motion of the anchors to i) move the payload, and ii) achieve the desired cables reconfiguration (internal motion). It is also interesting to compare this system to a classic cable driven parallel robot (CDPR). In a CDPR with fixed anchors, each cable is associated with only one degree of freedom, the cable length. The relation between motion of the payload and variations in the cable length is given by (see [11])

$$\dot{\boldsymbol{\rho}} = J\dot{\boldsymbol{x}} \,. \tag{14}$$

Clearly, for this system the degree of freedom (cable length) can only cause an instantaneous motion directed along the direction of the corresponding cable. Indeed, the kinematic relation (14) resembles (8) and in fact it is $J \equiv J_{\mathcal{R}}$.

IV. Dynamics

We introduce now the dynamics of both the payload and the quadrotors.

1) Payload: The dynamics of the cable suspended payload depend on few physical parameters, i.e., its total mass m_L, the position ${}^W\boldsymbol{c}_L = [c_x\, c_y\, c_z]^T \in \mathbb{R}^3$ of the center of mass in $\mathcal{F}_W$[5], and the 3×3 inertia matrix ${}^L J_L$ w.r.t. $\mathcal{F}_L$. Using the well known Newton-Euler or Euler-Lagrangian approaches, the payload dynamics is [11]

$$B_L(\boldsymbol{x_\nu})\ddot{\boldsymbol{x}} + C_L(\boldsymbol{x_\nu}, \dot{\boldsymbol{x}})\dot{\boldsymbol{x}} - \boldsymbol{g}_L(\boldsymbol{x_\nu}) = J_{\mathcal{R}}^T\boldsymbol{t} \,, \tag{15}$$

where $\boldsymbol{t} = [t_1,\ \ldots,\ t_m] \in \mathbb{R}^m$ is the vector of tensions of the cables, $J_{\mathcal{R}}^T\boldsymbol{t}$ is the wrench exerted on the payload by the cables, and B_L, C_L and $\boldsymbol{g}_L$ are defined as

$$B_L(\boldsymbol{x_\nu}) = \begin{bmatrix} m_L I_3 & m_L\,[{}^W\boldsymbol{c}_L]_\times{}^T \\ mL\,[{}^W\boldsymbol{c}_L]_\times & H_L \end{bmatrix}, \tag{16}$$

$$C_L(\boldsymbol{x_\nu}, \dot{\boldsymbol{x}})\dot{\boldsymbol{x}} = \begin{bmatrix} m_L\,[{}^W\boldsymbol{\omega}_L]_\times\,[{}^W\boldsymbol{\omega}_L]_\times\,{}^W\boldsymbol{c}_L \\ [{}^W\boldsymbol{\omega}_L]_\times\, H_L\,{}^W\boldsymbol{\omega}_L \end{bmatrix}, \tag{17}$$

$$\boldsymbol{g}_L(\boldsymbol{x_\nu}) = \begin{bmatrix} 0 & 0 & -m_L g & -m_L c_y g & m_L c_x g & 0 \end{bmatrix}^T, \tag{18}$$

$$H_L = {}^W R_L\,{}^L J_L\,{}^L R_W + m_L\,[{}^W\boldsymbol{c}_L]_\times\,[{}^W\boldsymbol{c}_L]_\times^T \,. \tag{19}$$

2) UAV: To model the 6 DoF (underactuated) dynamics of the i-th UAV connected to the cable we consider a north-west-up body frame $\mathcal{F}_{Q_i}$ that is attached to the center of mass A_i of the robot. The dynamics of the i-th UAV depend on its mass m_i and on the diagonal inertia matrix J_i w.r.t. the body frame, and have the well known form [12]

$$m_i\,{}^W\ddot{\boldsymbol{a}}_i = m_i g\boldsymbol{e}_3 + \tau_i\,{}^W R_{Q_i}\boldsymbol{e}_3 - {}^W\boldsymbol{n}_i t_i \tag{20}$$

$$J_i\dot{\boldsymbol{\omega}}_i = -\boldsymbol{\omega}_i \times J_i\boldsymbol{\omega}_i + \boldsymbol{\zeta}_i \tag{21}$$

where

- $\boldsymbol{w}_i$ is the angular velocity of the UAV in body frame;
- ${}^W R_{Q_i}$ is the rotation matrix of the body frame w.r.t. $\mathcal{F}_W$ and $\boldsymbol{e}_3 = [0\ 0\ 1]^T$;

[5]The position of the center of mass of the payload is typically expressed in $\mathcal{F}_L$ where it is constant, i.e., ${}^L\boldsymbol{c}_L$. Moving to $\mathcal{F}_W$ is straightforward, i.e. ${}^W\boldsymbol{c}_L = {}^W R_L\,{}^L\boldsymbol{c}_L$

- $-t_i {}^W\boldsymbol{n}_i$ is the reaction force applied by the cable on the UAV's center mass;
- J_i is the inertia matrix of the UAV w.r.t. $\mathcal{F}_{Q_i}$;
- $\tau_i \in \mathbb{R}$ is the thrust control input in body frame and $\boldsymbol{\zeta}_i \in \mathbb{R}^3$ is the attitude torque control input.

Remark 7. We can divide the linear dynamics of the i-th UAV into two components, parallel and orthogonal to the cable direction ${}^W\boldsymbol{n}_i$. With the same approach used in Sec. III, applying the projector operators $\pi_{\mathcal{R}} = {}^W\boldsymbol{n}_i {}^W\boldsymbol{n}_i^T$ and $\pi_{\mathcal{K}} = (I_{3\times 3} - {}^W\boldsymbol{n}_i {}^W\boldsymbol{n}_i^T)$ on (20) gives

$$\begin{aligned} m_i \pi_{\mathcal{R}} {}^W\ddot{\boldsymbol{a}}_i &= m_i g \pi_{\mathcal{R}} \boldsymbol{e}_3 + \tau_i \pi_{\mathcal{R}} {}^W R_{Q_i} \boldsymbol{e}_3 - {}^W\boldsymbol{n}_i t_i \\ m_i \pi_{\mathcal{K}} {}^W\ddot{\boldsymbol{a}}_i &= m_i g \pi_{\mathcal{K}} \boldsymbol{e}_3 + \tau_i \pi_{\mathcal{K}} {}^W R_{Q_i} \boldsymbol{e}_3 \end{aligned} \tag{22}$$

Equation (22) shows that the cable tension enters the linear dynamics of the UAV only along the cable direction. Namely, only the motion of the quadrotor along the cable applies a force on the payload, in accordance with spatial decomposition in Sec. III.

V. CONTROL

Assume now to have a desired payload trajectory $\boldsymbol{x}_{\boldsymbol{\nu},d}$, $\dot{\boldsymbol{x}}_d$ and $\ddot{\boldsymbol{x}}_d$, given by a planner or a human pilot, and the corresponding trajectory $\boldsymbol{\chi}_d$, $\dot{\boldsymbol{\chi}}_d$ and $\ddot{\boldsymbol{\chi}}_d$ for the anchors assigned from the kinematics (Sec. III). We must compute the inputs of the quadrotor such that the trajectories (of the payload and of the UAVs) are followed accurately and the tensions in the cables are feasible. To tackle this problem, we adopt a dual-space control approach with tension distribution akin to the controller presented in [13], [11] for a classic CDPR. This controller is composed by three elements: i) a control loop in task space that computes the wrench to be applied on the payload, ii) a tension distribution algorithm that optimally computes the cables tensions that achieve the desired wrench on the payload, and iii) a control loop in joint (UAVs) space that computes the inputs for the quadrotors subject to the required forces from the cables. These three steps are detailed in the following.

a) Task space: The loop in task space is implemented by using the following closed-loop inverse dynamics control,

$$\begin{aligned} \boldsymbol{f}_d &= B_L \ddot{\boldsymbol{z}} + C_L \dot{\boldsymbol{x}} - \boldsymbol{g}_L \\ \ddot{\boldsymbol{z}} &= \ddot{\boldsymbol{x}}_d + K_1 (\dot{\boldsymbol{x}}_d - \dot{\boldsymbol{x}}) + K_2 (\boldsymbol{x}_{\boldsymbol{\nu},d} - \boldsymbol{x}_{\boldsymbol{\nu}}) \end{aligned} \tag{23}$$

where K_1, K_2 are suitable diagonal matrices of positive gains. The vector $\boldsymbol{f}_d \in \mathbb{R}^6$ is the desired wrench applied to the payload, i.e.,

$$\boldsymbol{f}_d = J_{\mathcal{R}}^T \boldsymbol{t}. \tag{24}$$

b) Tension distribution: The required vector of tensions is computed by inverting (24). We recall (see [13]) that the tensions must be positive[6] and have a maximum value that depends on the cables themselves and on the actuation. Formally,

$$\boldsymbol{0} \leq \underline{\boldsymbol{t}} \leq \boldsymbol{t} \leq \bar{\boldsymbol{t}} \tag{25}$$

where $\underline{\boldsymbol{t}}$ is chosen high enough to prevent cable slackness, as in the hypothesis A2) in Sec. II. Here we simply assume that (24) is invertible and (25) is feasible. In practice this assumption can be guaranteed by restricting the payload and cables configurations to the so-called Wrench-Feasible-Workspace (WFW) [14], i.e. the set of configurations in which, for any wrench in a desired set there is a tensions vector that solves (24) and satisfies (25). Furthermore, provided that the required set of wrenches contains a neighborhood of the origin, $J_{\mathcal{R}}$ has full rank [15]. Note that for this system, the configurations considered to build the WFW include the pose of the payload and the cable directions N, as both are required to compute $J_{\mathcal{R}}$ (see (12)). If the number of cables is redundant w.r.t. the task, i.e., $m > n$, the solution to relation (24) is not unique but is found in a $n - m$ dimensional space, i.e.,

$$\boldsymbol{t}_d = \left(J_{\mathcal{R}}^T\right)^{\dagger} \boldsymbol{f}_d + Q\lambda, \tag{26}$$

where the superscript $\bullet^{\dagger}$ indicates the Moore-Penrose pseudoinverse, $Q \in \mathbb{R}^{m\times n-m}$ is a matrix whose columns span the null-space of $J_{\mathcal{R}}^T$ and $\boldsymbol{\lambda} \in \mathbb{R}^{n-m}$ is an arbitrary vector. The idea of tension distribution algorithms is to choose $\boldsymbol{\lambda}$ so as to optimize some criterium, i.e., to minimize the functional $1/2(\boldsymbol{t} - \boldsymbol{t}_m)^T(\boldsymbol{t} - \boldsymbol{t}_m)$ with $\boldsymbol{t}_m = (\bar{\boldsymbol{t}} + \underline{\boldsymbol{t}})/2$. The tension distribution problem can be solved by using one of the many methods known in literature, e.g., [16], [13].

c) Joint space: Given the trajectory $\boldsymbol{\chi}_d$, $\dot{\boldsymbol{\chi}}_d$ and $\ddot{\boldsymbol{\chi}}_d$ and the cable tension $\boldsymbol{t}_d$ (26), we implement the tracking controller for quadrotors that is detailed in [12]. This controller has an inner/outer loop structure. The slower outer loop position controller computes the thrust input and determines the desired roll and pitch commands as

$$\begin{aligned} \tau_i &= \frac{1}{\cos(\phi_i)\cos(\theta_i)} \Big(m_i \left[\ddot{\boldsymbol{y}}_i\right]_3 - m_i g - \left[{}^W\boldsymbol{n}_i \boldsymbol{t}_{d,i}\right]_3 \Big) \\ \begin{bmatrix} \sin(\theta_{i,d}) \\ \sin(\phi_{i,d}) \end{bmatrix} &= \frac{mT}{\tau_i} \Big(\left[\ddot{\boldsymbol{y}}_i\right]_{1:2} - \left[{}^W\boldsymbol{n}_i \boldsymbol{t}_{d,i}\right]_{1:2} \Big) \\ \ddot{\boldsymbol{y}} &= {}^W\ddot{\boldsymbol{a}}_{i,d} + k_1 \left({}^W\dot{\boldsymbol{a}}_{i,d} - {}^W\dot{\boldsymbol{a}}_i\right) + k_2 \left({}^W\boldsymbol{a}_{i,d} - {}^W\boldsymbol{a}_i\right) \end{aligned} \tag{27}$$

where ${}^W\boldsymbol{a}_i$ and ${}^W\boldsymbol{a}_{i,d}$ are the subvectors of $\boldsymbol{\chi}$ and $\boldsymbol{\chi}_d$ corresponding to the UAV (similar definitions for ${}^W\dot{\boldsymbol{a}}_i$, ${}^W\ddot{\boldsymbol{a}}_i$, etc.), $[\ddot{\boldsymbol{y}}]_{1:2}$ is the subvector of $\ddot{\boldsymbol{y}}$ formed by its first two components (analogous meaning for $[\ddot{\boldsymbol{y}}]_3$), k_1 and k_2 are positive gains, $\boldsymbol{\nu}_i = [\phi_i, \theta_i \psi_i]$ are the roll-pitch-yaw angles describing the orientation of the quadrotor in $\mathcal{F}_W$ and

$$T = \begin{bmatrix} \cos(\psi_i)/\cos(\phi_i) & \sin(\psi_i)/\cos(\phi_i) \\ \sin(\psi_i) & \cos(\psi_i) \end{bmatrix}$$

The faster inner loop attitude controller computes the torque input as

$$\boldsymbol{\zeta}_i = J_i \Big(- k_d \boldsymbol{\omega}_i + k_p E^{-1} (\boldsymbol{\nu}_{i,d} - \boldsymbol{\nu}_i) \Big) \tag{28}$$

where $\boldsymbol{\nu}_{i,d}$ are the desired roll-pitch-yaw angles, k_d, k_p are positive gains and $E(\boldsymbol{\nu})$ is the well known matrix that gives the mapping $\dot{\boldsymbol{\nu}} = E(\boldsymbol{\nu})\boldsymbol{\omega}_i$. The stability of the controller is proven in [12] for quasi-hovering configurations.

[6] Cables cannot push, but only pull.

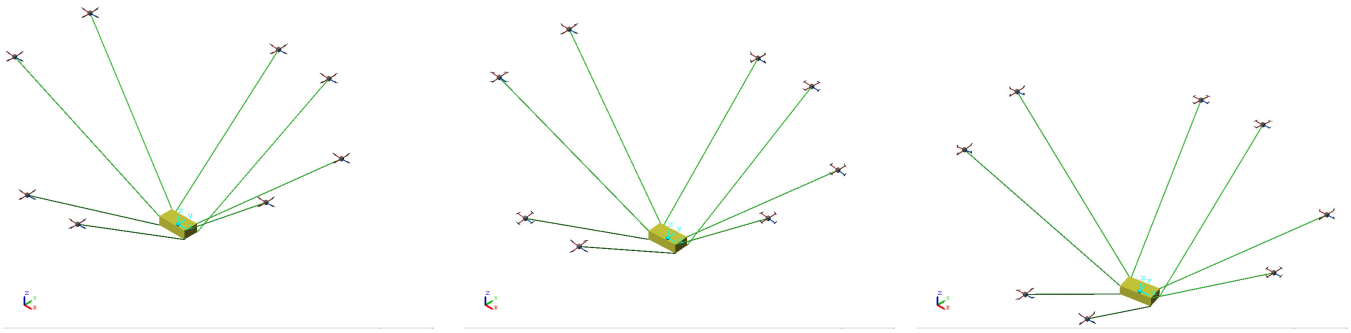

(a) Screenshot at $t = 0$ s.

(b) Screenshot at $t = 3$ s.

(c) Screenshot at $t = 5$ s.

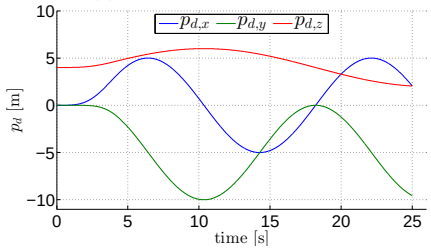

(d) Desired payload position.

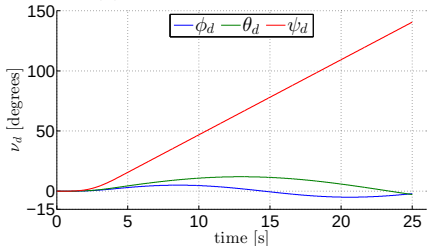

(e) Desired payload orientation

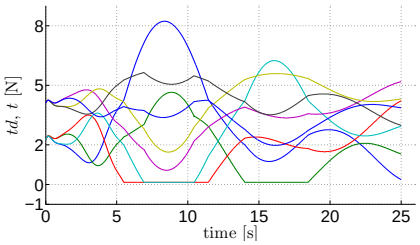

(f) Cable tensions after tension distribution.

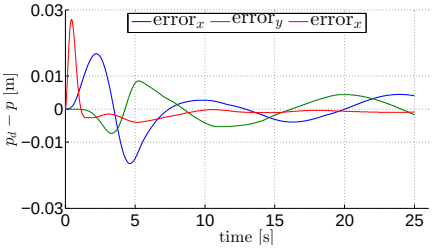

(g) Payload position error.

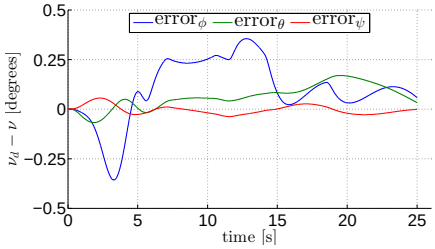

(h) Payload attitude error.

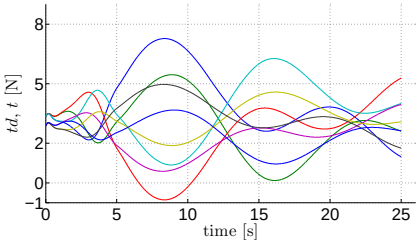

(i) Cable tensions with inversion $(J_{\mathcal{R}}^T)^\dagger \boldsymbol{f}_d$.

Fig. 3: Simulation 1

VI. EXPERIMENTS

We tested the proposed framework both in simulation and with real quadrotors. In these tests we implemented N and $\dot{N}$ according to two strategies as plausible examples of the functionalities achievable with the internal motions. These two strategies are the following:

Constant cable direction in $\mathcal{F}_L$: In this case the internal motion of the moving anchors is chosen such that the direction of the cables is fixed in the payload frame. This is a simple way to prevent collisions among the cables and to preserve the range of feasible wrenches, expressed in $\mathcal{F}_L$, that can be exerted on the payload[7]. In order to achieve this behaviour we impose that the cables rotate rigidly with the payload, i.e. for the generic i-th cable

$$\begin{aligned} {}^W\dot{\boldsymbol{n}}_i &= \boldsymbol{\omega} \times {}^W\boldsymbol{n}_i \\ {}^W\ddot{\boldsymbol{n}}_i &= \dot{\boldsymbol{\omega}} \times {}^W\boldsymbol{n}_i + \boldsymbol{\omega} \times {}^W\dot{\boldsymbol{n}}_i \end{aligned} \tag{29}$$

Formation shrinking/blooming: In this case the internal motion is designed to shrink (bloom) the formation by rotating the cables towards (away) from the vector $\boldsymbol{e}_3 = [0\ 0\ 1]^T$ in $\mathcal{F}_W$. This behaviour is implemented by choosing, for the i-th cable,

$$\begin{aligned} {}^W\dot{\boldsymbol{n}}_i &= \boldsymbol{\omega}_{\boldsymbol{n}_i} \times {}^W\boldsymbol{n}_i \\ {}^W\ddot{\boldsymbol{n}}_i &= \dot{\boldsymbol{\omega}}_{\boldsymbol{n}_i} \times {}^W\boldsymbol{n}_i + \boldsymbol{\omega}_{\boldsymbol{n}_i} \times {}^W\dot{\boldsymbol{n}}_i \\ \boldsymbol{\omega}_{\boldsymbol{n}_i} &= \alpha({}^W\boldsymbol{n}_i \times \boldsymbol{e}_3) \end{aligned} \tag{30}$$

where α can be chosen manually or it can be the result of a closed loop strategy.

A. Simulation

We first tested our approach in a physical simulation that has been developed using Simulink and SimMechanics. In the simulations we use $m = 8$ quadrotors to manipulate a cable suspended payload in the full $n = 6$ dimensional task space, thus resulting in two redundant cables that can be used to better distribute the tensions. To create the physical model of the system we implemented the assumption $A2$) from Sec. II by describing the cables as massless rigid links. We also impose $\underline{\boldsymbol{t}} = 0.1$ N and $\overline{\boldsymbol{t}} = 10$ N as limits for the cables tensions.

In the first simulation we command a predefined trajectory to the payload while the differential dynamics of the quadrotors are resolved by imposing (29). The screenshots 3a to 3c help visualizing how the payload moves in all the

[7]The wrench exerted on the payload and expressed in $\mathcal{F}_L$ depends on a matrix ${}^L J_{\mathcal{R}}^T$ that has the same structure presented in (12) but with all the vectors expressed in $\mathcal{F}_L$

6 degrees of freedom and how the quadrotors rearrange to keep the direction of the cables fixed w.r.t. the payload.

To look more in detail at the reference trajectory for the payload, we plot the position $\boldsymbol{p}_d$ and the orientation $\boldsymbol{\nu}_d$ in Figs. 3d and 3e, respectively. The tracking error of the payload when following these motion profiles is shown in Figs. 3g and 3h. We see that the tracking errors are kept very small during the whole task, validating the proposed approach. Finally we can compare the tensions $\boldsymbol{t}_d$ that are computed with the tension distribution (26) and without (by setting $\boldsymbol{\lambda} = \mathbf{0}_{2\times 1}$ in (26)). The tensions in these two cases are drawn in Figs. 3f and 3i, respectively. We can see that without tension distribution the forces required to the cables would become negative, and therefore unfeasible. On the other hand, the tension distribution not only distributes better the forces in the cables, but it also ensures that tensions never go below the minimum $\underline{t} = 0.1$N. Observe also see that at most two cables (exactly the number of redundant cables) have the minimum tension $\underline{t}$ at the same time.

In the second simulation the payload is commanded to stay in a fixed pose, while the internal motions are exploited to reconfigure the quadrotors. We impose the internal motion specified by (30) to shrink/expand the team of quadrotors. This behaviour is visible From the three dimensional trajectory of the quadrotors (see Fig. 4c) and from the screenshots 4a and 4b, where it is clear that the formation shrinks without moving the payload and that each robot moves on an arc centered on the corresponding connection point of the payload. The tracking error of the first quadrotor in following such a trajectory is presented in Fig. 4d. Finally, Fig. 4e shows the evolution of the tension vector $\boldsymbol{t}_d$ during the task. It stands out that reconfigurations of the team, even though they do not cause motions of the payload, affect the distribution of the cables tensions.

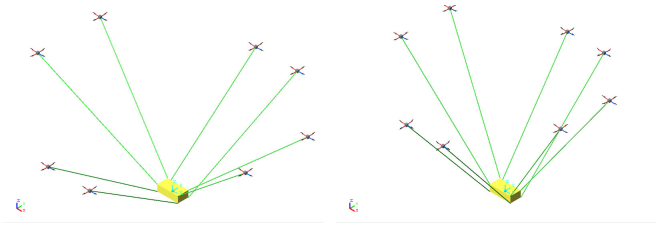

(a) Screenshot at $t = 0$ s. (b) Screenshot at $t = 5$ s.

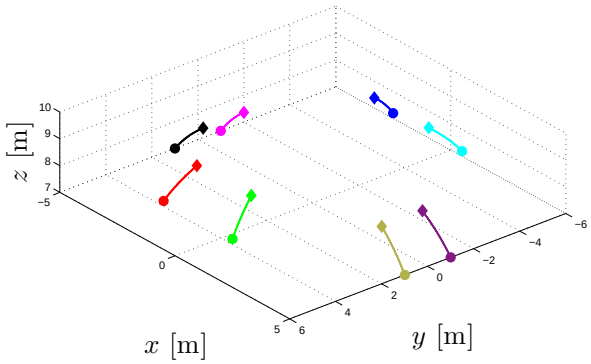

(c) Trajectories of the quadrotors.

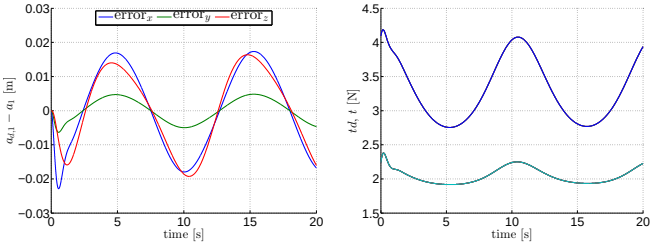

(d) Position error of quadrotor 1. (e) Cable tensions.

Fig. 4: Simulation 2

B. Experiment

We also tested our approach in a real experimental setting, using 4 quadrotors to transport a hollow box with dimensions $40 \times 31 \times 20$ cm and approximate mass of 0.5 kg (see **??**). The task considered in this example is to guide the payload along a trajectory specified on the $X - Y$ plane, while the remaining components of the pose of the payload are not controlled. With this choice the system has a redundancy equal to $n - m = 2$, which can be exploited to distribute the tensions along the cables. In alternative, one could also extend the task space to additionally command movements of the payload along the vertical direction or rotations. Lastly, we considered as limits for the cable tensions $\underline{t} = 0.1$ N and $\overline{t} = 5$ N.

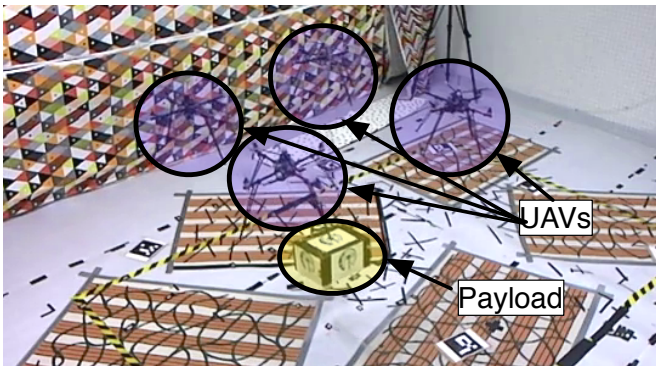

Fig. 5: Snapshot during the experiment.

In this experiment the reference trajectory for the payload is not predefined, but it is commanded online by a user through a joypad. In Simulink we implemented: 1) the differential kinematics algorithm that takes the reference trajectory for the payload and computes online the reference trajectory for the quadrotors; 2) the first two steps of the control strategy, i.e., the loop in the task space and the tension distribution. Finally, the reference trajectory for the quadrotors as well as the required cables tensions are sent via wireless serial communication to the UAV control layer that is onboard the quadrotors. The interface between Simulink and the serial channel is implemented using ROS and the Simulink Robotics Toolbox. This interface is also used to obtain from a Vicon tracking system the measurements of the states of the quadrotors and of the payload with a frequency of 120 Hz.

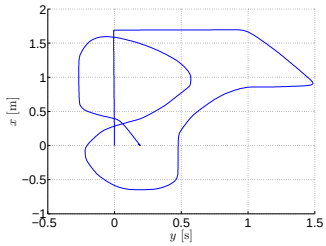

(a) Payload desired trajectory in XY plane.

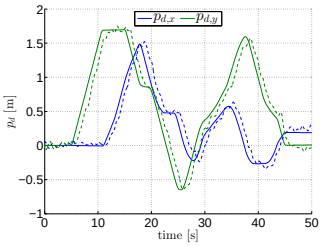

(b) Reference and actual position of the payload.

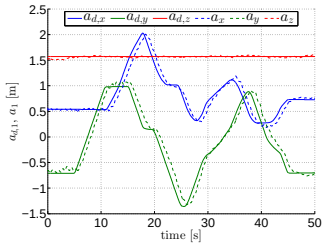

(c) Reference and actual position of quadrotor 1.

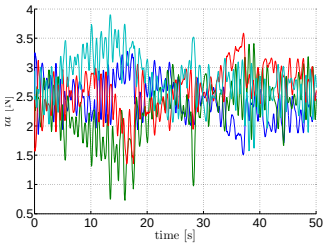

(d) Cable tensions using tension distribution.

Fig. 6: Results of the experiment.

Figure 6a shows the trajectory commanded to the payload by the user. The comparisons between commanded and executed motion for the payload and for a single quadrotor are shown in Figs. 6b and 6c respectively. In both cases it appears that the reference trajectory are followed quite well, but there is an evident delay. Indeed, during our experiments we experienced that the interface implemented through the Robotics Toolbox introduces a substantial communication delay and a slowdown on the Simulink model, limiting it to run in real time with a frequency of 20 Hz. As a consequence of these bottlenecks the motion of the quadrotors and of the payload showed some oscillations that are better visible from the companion video accompanying this paper. This phenomenon is also visible in the tension $\boldsymbol{t}_d$ required from the tension distribution and shown in Fig. 6d. Considering these problems and the fact that we have used a simple near-hovering controller without a closed control loop in the cables tensions, the tracking of the trajectories shown in Figs. 6b and 6c is very satisfactory.

VII. CONCLUSIONS

In this paper we have presented a novel solution to the problem of cooperative aerial transportation of a suspended payload using quadrotors. In comparison to previous works on this topic we addressed the problem from a different perspective, i.e. looking to find a direct and intuitive kinematic relation between the motion of the payload and the motion of the quadrotors. By doing so, we have found a description that is general (can be applied to other RCDPR), is very intuitive, does not require pre-planning of the forces and is suitable for a teleoperation framework. We are now planning to further develop this framework in several directions. In particular, we want to research 1) ways to use the internal motions to achieve various task, both automatically or under the command of a user, 2) a decentralized implementation of the approach, 3) a new design for a quadrotor to improve the cable connection and to make the robot more capable of exerting forces.

REFERENCES

[1] N. Michael, S. Kim, J. Fink, and V. Kumar, "Kinematics and statics of cooperative multi-robot aerial manipulation with cables," in *ASME Int. Design Engineering Technical Conf.*, 2009.

[2] N. Michael, J. Fink, and V. Kumar, "Cooperative manipulation and transportation with aerial robots," *Autonomous Robots*, vol. 30, no. 1, pp. 73–86, 2011.

[3] J. Fink, N. Michael, S. Kim, and V. Kumar, "Planning and control for cooperative manipulation and transportation with aerial robots," *The International Journal of Robotics Research*, vol. 30, no. 3, pp. 324–334, 2011.

[4] I. Maza, K. Kondak, M. Bernard, and A. Ollero, "Multi-UAV cooperation and control for load transportation and deployment," *Journal of Intelligent & Robotics Systems*, vol. 57, no. 1-4, pp. 417–449, 2010.

[5] M. Bernard, K. Kondak, I. Maza, and A. Ollero, "Autonomous transportation and deployment with aerial robots for search and rescue missions," *Journal of Field Robotics*, vol. 28, no. 6, pp. 914–931, 2011.

[6] K. Sreenath and V. Kumar, "Dynamics, control and planning for cooperative manipulation of payloads suspended by cables from multiple quadrotor robots," in *Robotics: Science and Systems*, 2013.

[7] X. Zhou, C. Tang, and V. Krovi, "Cooperating mobile cable robots: Screw theoretic analysis," in *Redundancy in Robot Manipulators and Multi-Robot Systems*, ser. Lecture Notes in Electrical Engineering, D. Milutinovic and J. Rosen, Eds. Springer Berlin Heidelberg, 2013, vol. 57, pp. 109–123.

[8] D. Nguyen, M. Gouttefarde, O. Company, and F. Pierrot, "On the analysis of large-dimension reconfigurable suspended cable-driven parallel robots," in *2014 IEEE Int. Conf. on Robotics and Automation*, May 2014, pp. 5728–5735.

[9] D. Nguyen and M. Gouttefarde, "Study of reconfigurable suspended cable-driven parallel robots for airplane maintenance," in *2014 IEEE/RSJ Int. Conf. on Intelligent Robots and Systems*, Sept. 2014, pp. 1682–1689.

[10] L. Gagliardini, S. Caro, M. Gouttefarde, P. Wenger, and A. Girin, "A reconfigurable cable-driven parallel robot for sandblasting and painting of large structures," in *Cable-Driven Parallel Robots*, ser. Mechanisms and Machine Science, A. Pott and T. Bruckmann, Eds. Springer International Publishing, 2015, vol. 32, pp. 275–291.

[11] J. Lamaury, M. Gouttefarde, A. Chemori, and P.-E. Herve, "Dual-space adaptive control of redundantly actuated cable-driven parallel robots," in *2013 IEEE/RSJ Int. Conf. on Intelligent Robots and Systems*, Nov 2013, pp. 4879–4886.

[12] D. Lee, A. Franchi, H. I. Son, H. H. Bülthoff, and P. Robuffo Giordano, "Semi-autonomous haptic teleoperation control architecture of multiple unmanned aerial vehicles," *IEEE/ASME Trans. on Mechatronics, Focused Section on Aerospace Mechatronics*, vol. 18, no. 4, pp. 1334–1345, 2013.

[13] J. Lamaury and M. Gouttefarde, "Control of a large redundantly actuated cable-suspended parallel robot," in *2013 IEEE Int. Conf. on Robotics and Automation*, May 2013, pp. 4659–4664.

[14] P. Bosscher and I. Ebert-Uphoff, "Wrench-based analysis of cable-driven robots," in *2004 IEEE Int. Conf. on Robotics and Automation*, vol. 5, April 2004, pp. 4950–4955.

[15] M. Gouttefarde, D. Daney, and J. Merlet, "Interval-analysis-based determination of the wrench-feasible workspace of parallel cable-driven robots," *IEEE Trans. on Robotics*, vol. 27, no. 1, pp. 1–13, Feb 2011.

[16] L. Mikelsons, T. Bruckmann, M. Hiller, and D. Schramm, "A real-time capable force calculation algorithm for redundant tendon-based parallel manipulators," in *2008 IEEE Int. Conf. on Robotics and Automation*, May 2008, pp. 3869–3874.